Available online at www.sciencedirect.com
SCIENCE DIRECT®
Journal of Sound and Vibration 266 (2003) 235–260
JOURNAL OF SOUND AND VIBRATION
www.elsevier.com/locate/jsvi

Dynamic sensitivity analysis for the pantograph of a high-speed rail vehicle

Tong-Jin Park[a], Chang-Soo Han[b,*], Jin-Hee Jang[c]

[a] *Department of Precision Mechanical Engineering, Hanyang University, South Korea*
[b] *Division of Mechanical Engineering, Hanyang University, Sa 1 dong, 1271, Ansan, Kyonggi-do 425-791, South Korea*
[c] *Technical Research Center, Daewoo Motors, South Korea*

Received 9 April 2002; accepted 10 September 2002

Abstract

In this study, the dynamic characteristics of a catenary system using the finite element method (FEM) and dynamic modelling for developing a suitable pantograph at high speed is analyzed. First, the catenary system of a high-speed railway is assumed to be a beam model. Next, an analysis program using finite element analysis was performed. The pantograph of linear spring–mass system is assumed to be three-degrees-of-freedom model for the finite element analysis. The analyses of the catenary based on the FEM are executed to develop a pantograph that meets the necessary standards for high-speed rail vehicles. Using a simulation of the pantograph–catenary system, the static deflection of the catenary, the stiffness variation in the contact lines, the dynamic response of the catenary undergoing a constant moving load and the contact force analysis were executed. From the pantograph–catenary analysis, the design parameters of a pantograph could be optimized. Based on the design-parameter analysis, a pantograph with improved parameters was found to be suitable for a high-speed rail vehicle.

1. Introduction

At present, the high-speed railway that is focused on as the next generation transportation system is characterized by high stability, high driving velocity and comfort, all of which are uncommon foci of other transportation systems. An accompanying problem of the high speed of the railway is ensuring stable current collection. For stable operation of a railway, the catenary must be supplied with stable electrical power through solid contact with the pantograph. If the railway speed is increased, the width of the catenary's dynamical variation will increase. Contact

*Corresponding author. Tel.: +82-31-400-5247; fax: +82-31-406-6242.
E-mail address: djpark@ihanyang.ac.kr, cshan@hanyang.ac.kr (C.-S. Han).

0022-460X/03/$ - see front matter © 2002 Elsevier Science Ltd. All rights reserved.
doi:10.1016/S0022-460X(02)01280-4

loss will then occur between the pantograph and the catenary. In addition, wear on the pantograph is going to grow as electrical shock and damage occur [11]. Therefore, research for understanding the current-collecting system's dynamic characteristics and the decreasing width of dynamic variation are needed. Progress has been made in research for assuring the ability of high-speed driving as basic technology of a high-speed railway [3,9]. Ockendon and Taylor described an approximate analytical formulation to determine contact force [12]. Manabe conducted research on wave analyses to study the response between the pantograph and the catenary with discrete support springs [6]. Wu and Brennan investigated the dynamic relation using the finite element method (FEM) between the catenary and the pantograph [7]. Vinayagalingam studied contact force variation and panhead trajectory by using finite difference methods [10]. Today's situation is that an active pantograph is proposed for more stable current collection through maximizing the ability of the pantograph to follow the catenary [2–5].

To improve the performance of the pantograph, its dynamics should be more considered before applying active system. Especially, many researchers for improving the system performance have been suggested using sensitivity analysis as an efficient tool for checking variations in design variables based on its dynamics. Vanderplaats and Arora found that sensitivity information can be used as a design basis when re-designing a system [13,14]. Haug et al. investigated dynamic sensitivity analysis, which is utilized for variation evaluation of mechanisms in the dynamic state [12]. Jang and Han devised a way to conduct dynamic sensitivity analyses for studying state sensitivity information with respect to changes in design variables [1]. Therefore, sensitivity analysis is useful tool for improving dynamic characteristics of a pantograph.

The output of the pantograph system analyzed by catenary dynamics and pantograph dynamics is contact force between catenary and pantograph as the ability of the stable current collection of the pantograph can be determined by contact force. The objective of this research is to study state sensitivity information for contact force with respect to changes in the design variables on pantograph.

In this study, the catenary system of a high-speed railway was assumed to be a beam model. Using FEM for analyzing a high-speed rail pantograph the catenary dynamics is organized for a total of 10 spans and analyzed for confirming contact force more than 350 km/h. The pantograph of a linear spring–mass system is assumed to be a three-degrees-of-freedom model (t.d.o.f.) model. In sensitivity analysis, the direct differentiation method is used. Finally, the dominant design variables of the system are suggested via analysis and trends for the redesign of the pantograph are proposed.

2. Modelling of the catenary and the pantograph

Three types of centenary systems can be used in a high-speed railway—simple, stitched and compound. The reason for having various types of catenaries is to unify the mechanical characteristics of the contact wire contacting the pantograph.

2.1. Modelling of the catenary system

Fig. 1 shows the structure of a simple catenary system.

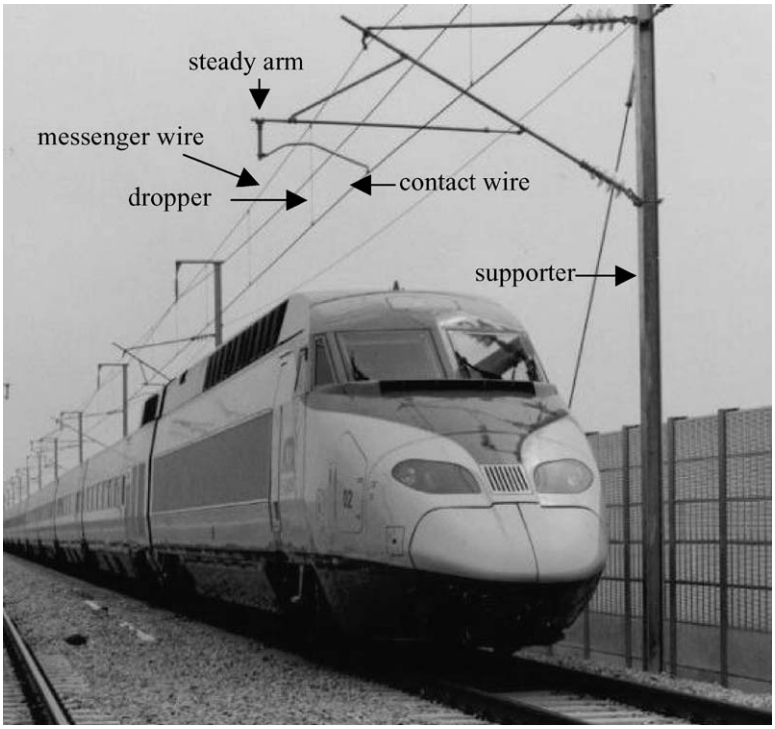

Fig. 1. Structure of a simple catenary system of a high-speed rail vehicle.

The contact wire is the supplier of current through direct contact with the pantograph on the roof of the train. The contact wire must adjust to the distance between the catenary and the railroad. For mathematical modelling, a tensioning beam considering the high-frequency response component is proposed. The messenger wire supports the contact wire for sustaining a flexible distance from the track-suspending supporter. In this study, a messenger wire tension beam that is given definite tension force similar to the contact wire is proposed. The dropper is the cable which spreads the dynamic mass applied to the contact wire and which connects the contact wire with the messenger wire to keep the contact wire from touching the messenger wire. Therefore, the dropper is modelled as the mass and spring. At present, the dropper is set up with nine pieces per 63 m span. The interval of each dropper is 4.5 m in the vicinity of the supporter, the others are at intervals of 6.75 m. The dropper plays the important role of maintaining uniform height and equal elasticity for the contact wire. The steady arm is the element that permits stagger for preventing the contact wire from being worn on one side through continuous contact with one point of the pantograph. The distance between each supporter is one unit of span. Its role is to push and pull the contact wire horizontally. The steady arm is modelled as mass and spring in the contact wire. The supporter, that is a messenger wire supported by a column, can be considered as a cantilever when it is modelled. Similarly, with the steady arm, the supporter can be modelled as equal mass and spring. The space between two supports is one span, and generally, each support is set at intervals of 63 m.

First, the motion of the equation of the messenger wire can be expressed as

$$m_m \frac{\partial^2 u_m}{\partial t^2} + \frac{\partial^2}{\partial x^2}\left(EI_m \frac{\partial^2 u_m}{\partial x^2}\right) - \frac{\partial}{\partial x}\left(T_m \frac{\partial u_m}{\partial x}\right) + k_d(u_m - u_c)\delta(x - x_n) + k_s u_m \delta(x - x_s) = 0, \quad (1)$$

where m_m, T_m, and EI_m express the unit mass of the messenger wire, tension force, and bending stiffness, respectively, k_d is the stiffness of the dropper, and expresses the relevant force in relation to the contact wire on the position of droppers. k_s expresses the equivalent stiffness of the supporter.

The motion of equation of the contact wire can be expressed as

$$m_c \frac{\partial^2 u_c}{\partial t^2} + \frac{\partial^2}{\partial x^2}\left(EI_c \frac{\partial^2 u_c}{\partial x^2}\right) - \frac{\partial}{\partial x}\left(T_c \frac{\partial u_c}{\partial x}\right) - k_d(u_m - u_c)\delta(x - x_n) = P\delta(x - Vt), \quad (2)$$

where m_c, T_c, and EI_c express the unit mass of the contact wire, tension force, and bending stiffness, respectively. δ is the delta function, and P is the contact force that is forced from the pantograph to the contact wire. P is the function for time space. Motion of the equation for the catenary is related to contact force. The contact wire and the messenger wires are connected to each other. As a result the equation cannot be solved easily.

In this study, displacement of the catenary is obtained each time with the numerical analysis using FEM. Using FEM, the catenary system can be solved analytically. However, the results of FEM are from the view point of the catenary system with constructive dynamics. The catenary system should be simplified for solving the pantograph dynamics from FEM. In this study, the catenary system response is regarded as a stiffness function by the stiffness distribution from the FEM. This approach has been investigated by many researchers. Wu [8] investigated the function of the dynamic stiffness based on the catenary modelling. Balestrino et al. [2] derived the mass, stiffness and damper functions of the catenary system from the experimental results. The aim of the stiffness function is to simplify the pantograph system in time domain. To obtain the dynamic response of the combined catenary and pantograph system, the catenary, that is a continuous system, needs to be modelled as a spring with varying stiffness according to the position in a span. The mass of the catenary that affects dynamic response of the combined catenary–pantograph system are weak [2]. Therefore, the mass of the catenary is neglected in this study.

The three-span catenary is modelled as shown in Fig. 2 to obtain vertical stiffness along the span of the catenary. The stiffness matrix is constructed using FEM. The catenary wire is considered as beam a element. Then, an arbitrary force, that is, the uplift force of pantograph, is given to one point of the middle span of the catenary. The first and the third span of the catenary are only used to give continuity to the middle span and to avoid fixed boundary conditions. The vertical stiffness of that point is the value of the force divided by the displacement.

Stiffness values derived are discontinuous between nodal points. Therefore, they should be described using equivalent continuous functions for simulations. The equivalent functions are obtained by using the maximum and minimum stiffness values and one span length. The equivalent functions of stiffness related to position x along the catenary span are represented by the following equations:

$$K(x) = K_0\left(1 - \alpha \cos\frac{2\pi x}{L}\right), \quad (3)$$

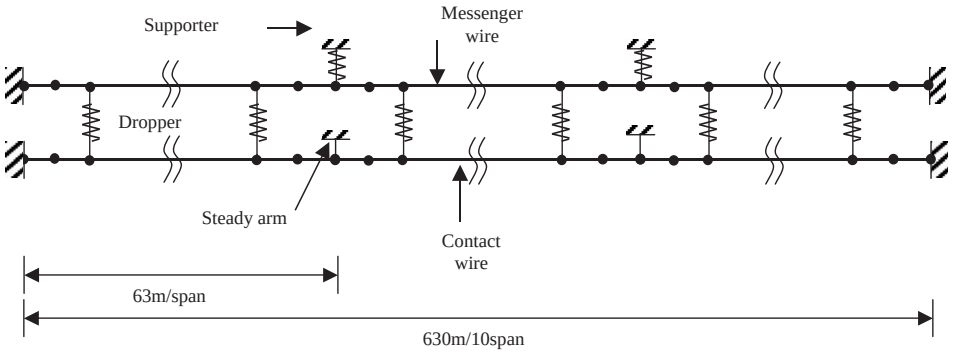

Fig. 2. Three span catenary system modelling using FEM.

Table 1
Equivalent functions of the stiffness of each span

L (m)	K_0 (N/m)	α	$K(x)$
40.5	2435.6	0.1256	$2435.6(1-0.1256\cos 0.155x)$
45	2172	0.0823	$2172(1-0.0823\cos 0.14x)$
49.5	2126.6	0.1247	$2126.6(1-0.1247\cos 0.127x)$
63	1916.7	0.1776	$1916.7(1-0.1776\cos 0.1x)$

where

$$K_0 = \frac{K_{max} + K_{min}}{2}, \quad \alpha = \frac{K_{max} - K_{min}}{K_{max} + K_{min}}.$$

K_{max} and K_{min} are the maximum and minimum stiffness values and L is one span length. The equivalent functions of the catenary stiffness obtained by Eq. (3) are represented in Table 1 and the equivalent functions are described by Fig. 3.

The solid line is the FEM result; the others are the approximated functions of catenary stiffness. The stiffness of the catenary at time t that is touched by an object traveling at speed V can be written as follows:

$$K(t) = K_0\left(1 - \alpha\cos\frac{2\pi V}{L}t\right), \tag{4}$$

where

$$K_0 = \frac{K_{max} + K_{min}}{2}, \quad \alpha = \frac{K_{max} - K_{min}}{K_{max} + K_{min}}.$$

Eq. (4) is the stiffness function of the caterary system by velocity and time. The contact force between the catenary and the pantograph is derived by Eq. (4). For sensitivity analysis, the approximated catenary system as a stiffness function is suitable because catenary is acting as an external force input in pantograph dynamics. The stiffness, $K(t)$, is used as the dynamic variable of the pantograph for the contact force in this study.

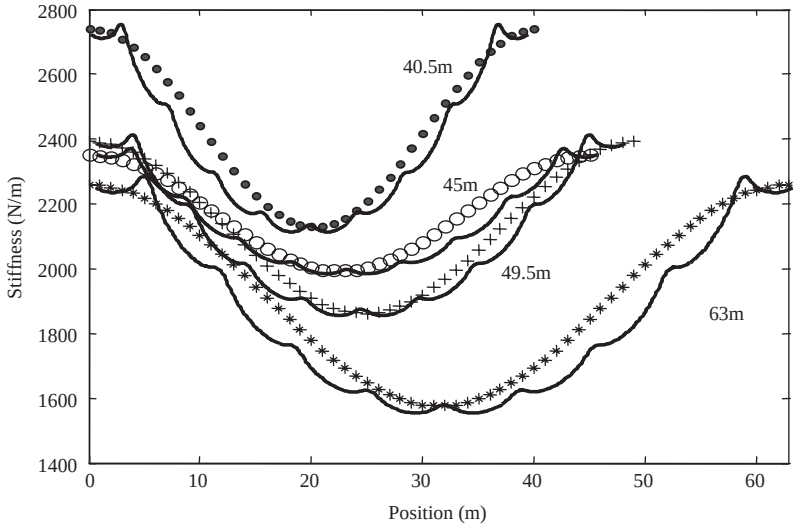

Fig. 3. Catenary stiffness functions by 1 span.

2.2. Modelling of the pantograph

Contact loss determined by analyzing the contact force is an important factor for establishing the dynamic design variables of the pantograph.

Contact loss with the catenary system occurred as follows:

- Wave propagation and elasticity irregularity.
- Stiffness variation at dropper connection points.
- Minimal unevenness at the connecting surface of the contact wire.
- Mass variation at the part of the steady arm for support and connection.
- Variation of coach vibration and wind pressure from outside the train.

Analyzing contact loss under these conditions, the pantograph should be modelled for satisfying performance as follows:

- Ability of the stable current collection at a high speed.
- Quick reaction ability for variation of characteristic variables.
- Low deviation of vibration for the pantograph–catenary system at high speed.

For satisfying performance, the pantograph is of the GPU (large single plunger) type high-speed rail. Fig. 4 shows the GPU pantograph.

Fig. 5 shows the dynamic modelling from the GPU pantograph.

In Fig. 5, the pantograph model is composed of a three lumped mass, a spring, a damper, a friction damper between each mass, and the structure that supplies external force for each mass. The t.d.o.f. pantograph modelling is defined in Fig. 2. The motion equation is derived at each

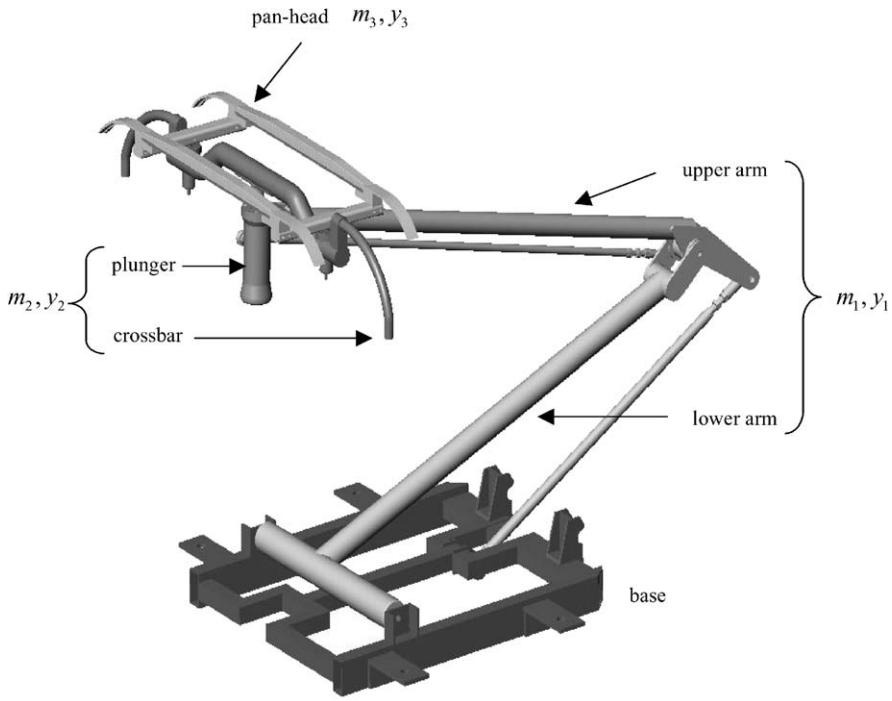

Fig. 4. GPU pantograph.

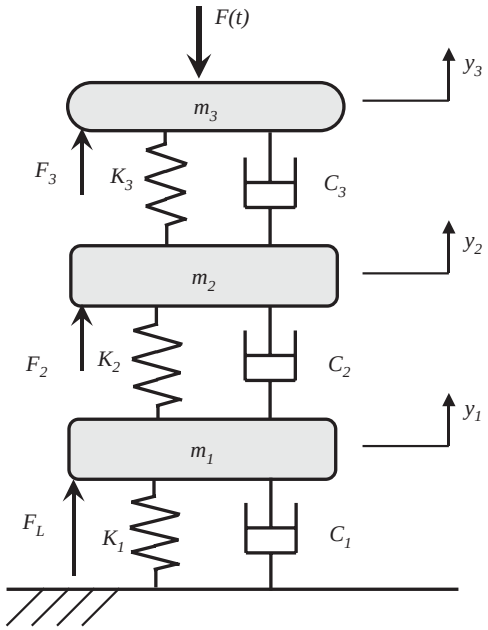

Fig. 5. Pantograph dynamic modelling.

nodal point

$$m_3\ddot{y}_3 - c_3\dot{y}_2 - k_3y_2 + c_3\dot{y}_3 + k_3y_3 = -P(t) + F_3, \tag{5}$$

$$m_2\ddot{y}_2 - c_2\dot{y}_1 - k_2y_1 + (c_2 + c_3)\dot{y}_2 + (k_2 + k_3)y_2 - c_3\dot{y}_3 - k_3y_3 = F_2, \tag{6}$$

$$m_1\ddot{y}_1 + (c_1 + c_2)\dot{y}_1 + (k_1 + k_2)y_1 - c_2\dot{y}_2 - k_2y_2 = F_L, \tag{7}$$

where F_3 and F_2 are lift forces by aero force at high speeds. F_L is lift force of the base to contact the caternary system. $P(t)$ is the contact force between the pantograph and catenary. It is most important to know the contact force between the contact wire and the panhead of the pantograph and in determining the magnitude of the contact force and the displacement of the contact wire at the contact point, the phenomenon that occurs during high-speed driving can be easily analyzed. According to the magnitude of the contact force, the design values of the pantograph can be determined.

From Eq. (4), the contact force is derived from the stiffness of the catenary system only. Using Eq. (4) the contact force is as follows:

$$P(t) = K(t)y_3 = K_0\left(1 - \alpha\cos\frac{2\pi V}{L}t\right)y_3. \tag{8}$$

Eq. (8) calculates contact force by varying as vehicle velocity. In sensitivity analysis, y_3 is also affected by contact force from the catenary stiffness function. Eq. (5) is modified as follows:

$$m_3\ddot{y}_3 - c_3\dot{y}_2 - k_3y_2 + c_3\dot{y}_3 + (k_3 + K(t))y_3 = F_3. \tag{9}$$

Eq. (9) is the relation between the panhead and the catenary. The pantograph system is a linear system itself; however, as the catenary stiffness function for varying as time is added to pantograph dynamics, the pantograph system equation is a linear time varying system.

2.3. Validation of pantograph modelling

For sensitivity analysis, pantograph modelling should be investigated by experimental results. The experimental equipment vibrated on the panhead with the same frequencies and displacements as the behavior of a high-speed rail system. From Eq. (4), considering the length of supporters, L, and vehicle velocity, V, in cosine function, the frequency from 8 to 17 Hz is regarded as a high frequency caused by speeds more than 350 km/h. For example, if L is 63 m and V is 350 km/h, then frequency, ω is 9.8 Hz assuming as $\omega = 2\pi V/L$. The vibration experiments measured the acceleration of the panhead, crossbar, and plunger. Fig. 6 shows the vibration experiments of the pantograph.

The acceleration signals using the spectrum analysis were compared with the modelling in the frequency domain.

Figs. 7–9 show the comparisons between the experiments and modelling under 6.1, 9.8 and 14.3 Hz. Comparing the experiments and modelling, the frequency was almost exact, and the amplitude has some error for the experiment. From these results, the pantograph modelling is valid for sensitivity analysis.

Fig. 6. Pantograph vibration experiment.

3. Sensitivity formulation

In order to perform sensitivity analysis, state sensitivity equations must be derived with respect to the design variables at the initial stage. In this study, the state variables of the system are as follows:

$$\mathbf{z} = \begin{bmatrix} y_1 & \dot{y}_1 & y_2 & \dot{y}_2 & y_3 & \dot{y}_3 \end{bmatrix}^{\mathrm{T}}, \tag{10}$$

where $\mathbf{z}$ is the state variable vector, y and $\dot{y}$ are displacements and velocities of each mass, respectively. Design variables of this system are selected as

$$\begin{aligned} \mathbf{b} &= \begin{bmatrix} b_1 & b_2 & b_3 & b_4 & b_5 & b_6 & b_7 & b_8 & b_9 \end{bmatrix}^{\mathrm{T}} \\ &= \begin{bmatrix} m_1 & m_2 & m_3 & c_1 & c_2 & c_3 & k_1 & k_2 & k_3 \end{bmatrix}^{\mathrm{T}}. \end{aligned} \tag{11}$$

The dynamic equations of motion for the pantograph system can be expressed in the following form:

$$\dot{\mathbf{z}} = \begin{bmatrix} \dot{y}_1 \\ \dfrac{-(k_1+k_2)y_1}{m_1} - \dfrac{(c_1+c_2)\dot{y}_1}{m_1} + \dfrac{k_2 y_2}{m_1} + \dfrac{c_2\dot{y}_2}{m_1} + \dfrac{F_L}{m_1} \\ \dot{y}_2 \\ \dfrac{k_2 y_1}{m_2} + \dfrac{c_2\dot{y}_1}{m_2} - \dfrac{(k_2+k_3)y_2}{m_2} - \dfrac{(c_2+c_3)\dot{y}_2}{m_2} + \dfrac{k_3 y_3}{m_2} + \dfrac{c_3\dot{y}_3}{m_2} + \dfrac{F_2}{m_2} \\ \dot{y}_3 \\ \dfrac{k_3 y_2}{m_3} + \dfrac{c_3\dot{y}_2}{m_3} - \dfrac{(k_3+K(t))y_3}{m_3} - \dfrac{c_3\dot{y}_3}{m_3} + \dfrac{F_3}{m_3} \end{bmatrix}. \tag{12}$$

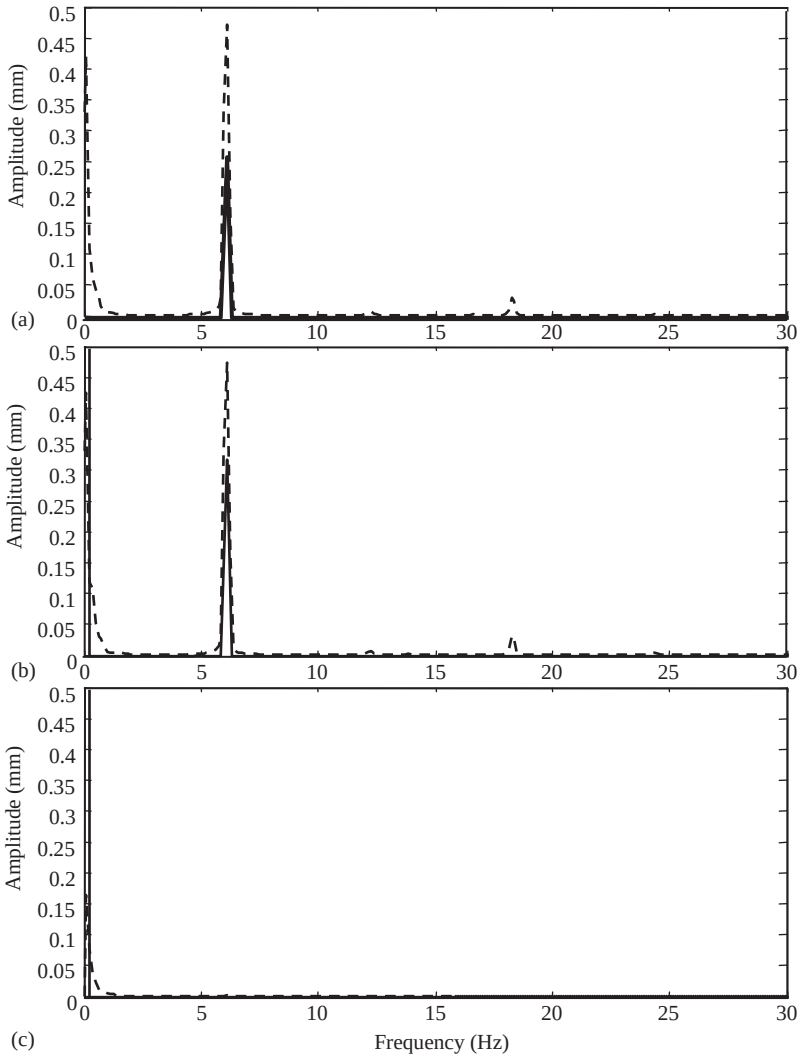

Fig. 7. Frequency spectrums at 6.1 Hz, 0.5 mm excitation. Experiment (- - -) and modelling (—); (a) panhead amplitude (mm); (b) crossbar amplitude (mm); and (c) plunger amplitude (mm).

This equation has the form of a first order ordinary differential equation. In order to perform sensitivity analysis, state sensitivity equations must be derived with respect to the design variables at the initial stage. A general form of the first order differential sensitivity equations is

$$\frac{\partial \dot{\mathbf{z}}}{\partial \mathbf{b}} = \frac{\partial \mathbf{f}}{\partial \mathbf{z}} \cdot \frac{\mathrm{d}\mathbf{z}}{\mathrm{d}\mathbf{b}} + \frac{\partial \mathbf{f}}{\partial \mathbf{b}}. \tag{13}$$

This equation can be written in the following compact matrix from:

$$\dot{\mathbf{z}}_b = \mathbf{f}_z \cdot \mathbf{z}_b + \mathbf{f}_b, \tag{14}$$

where $\mathbf{z} \in \mathbf{R}^n, \mathbf{b} \in \mathbf{R}^n, \mathbf{f} \in \mathbf{R}^n$, $\mathbf{z} \in \mathbf{R}^{n \times m}$, $\mathbf{f}_z \in \mathbf{R}^{n \times n}$, and $\mathbf{f}_b \in \mathbf{R}^{n \times m}$.

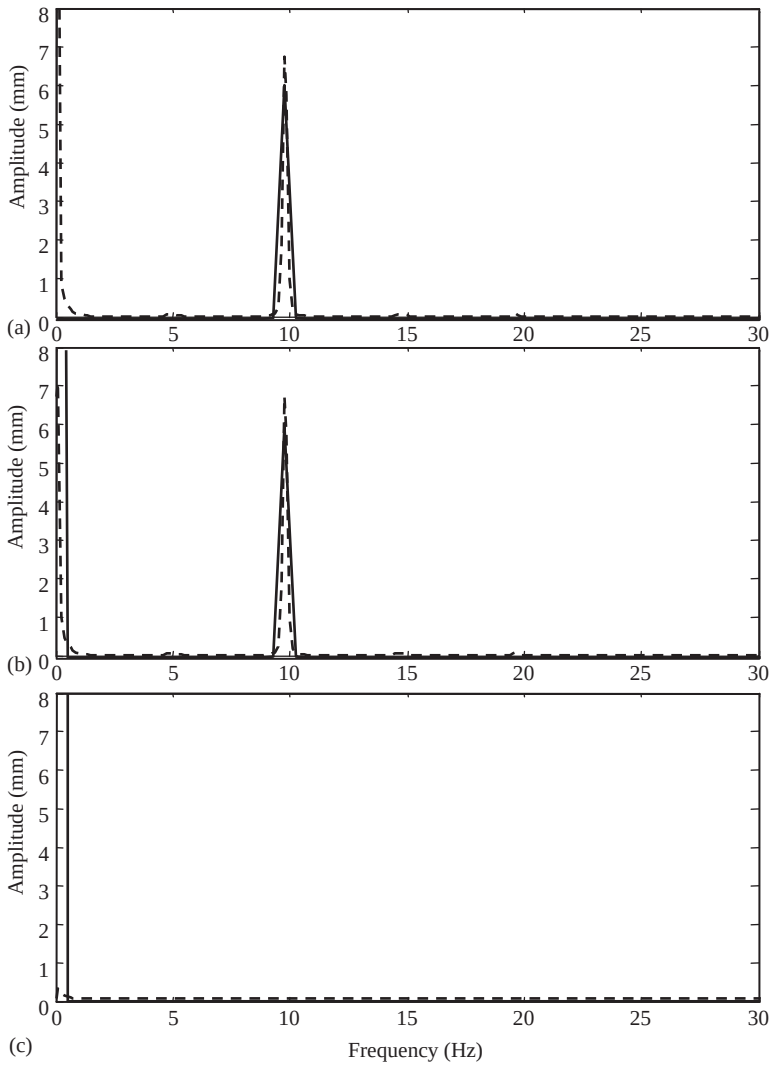

Fig. 8. Frequency spectrum at 9.8 Hz, 3.48 mm excitation. Experiment (- - -) and modelling (—); (a) panhead amplitude (mm); (b) crossbar amplitude (mm); and (c) plunger amplitude (mm).

n is the number of state variables and m is the number of design variables. In this case, n is 6 and m is 9 from Eq. (12). $\mathbf{z}_b$ is state sensitivity matrix with respect to the design variables and $\dot{\mathbf{z}}_b$ is the time derivative of the state sensitivity matrix. For linear different equations, $\mathbf{f}_z$ can be expressed by system matrix $\mathbf{A}$. From this idea, Eq. (14) can be re-written in the following form:

$$\dot{\mathbf{z}}_b = \mathbf{A} \cdot \mathbf{z}_b + \mathbf{f}_b. \tag{15}$$

Next, $\mathbf{f}_b$ should be obtained from the last term of the state sensitivity analysis with respect to the design variables; this term is expressed in following matrix form:

$$\mathbf{f}_b = [\mathbf{f}_{b1}, \mathbf{f}_{b2}, \mathbf{f}_{b3}, \mathbf{f}_{b4}, \mathbf{f}_{b5}, \mathbf{f}_{b6}, \mathbf{f}_{b7}, \mathbf{f}_{b8}, \mathbf{f}_{b9}]_{6\times 9}. \tag{16}$$

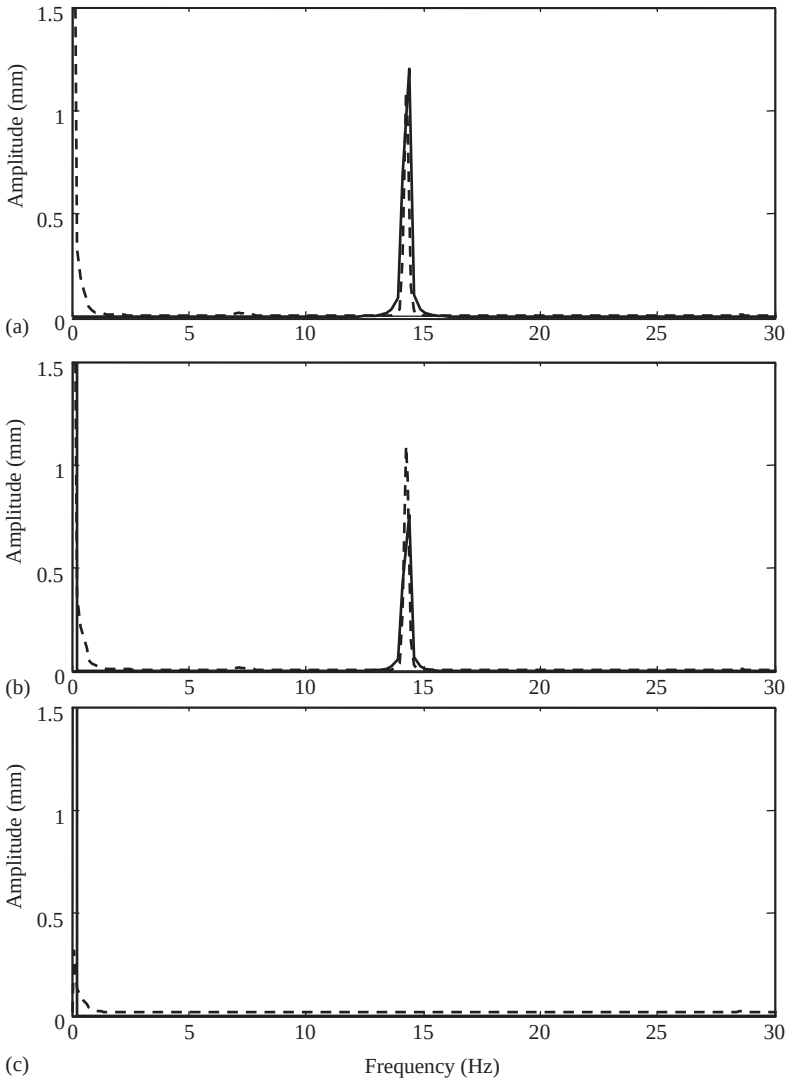

Fig. 9. Frequency spectrum at 14.3 Hz, 1.5 mm excitation. Experiment (- - -) and modelling (—); (a) panhead amplitude (mm); (b) crossbar amplitude (mm); and (c) plunger amplitude (mm).

Detailed derivations of the above are summarized in Appendix A. In order to solve the dynamic and state sensitivity equations of the system, Eqs. (12) and (15) are simultaneously integrated.

4. Results of the sensitivity analysis

Various sensitivity analyses of the pantograph–catenary system are performed in the time domain. In this study, sensitivity is evaluated for the contact force at various speeds (100–400 km/h). The effects of the design variables of the pantograph on state sensitivity are examined and a

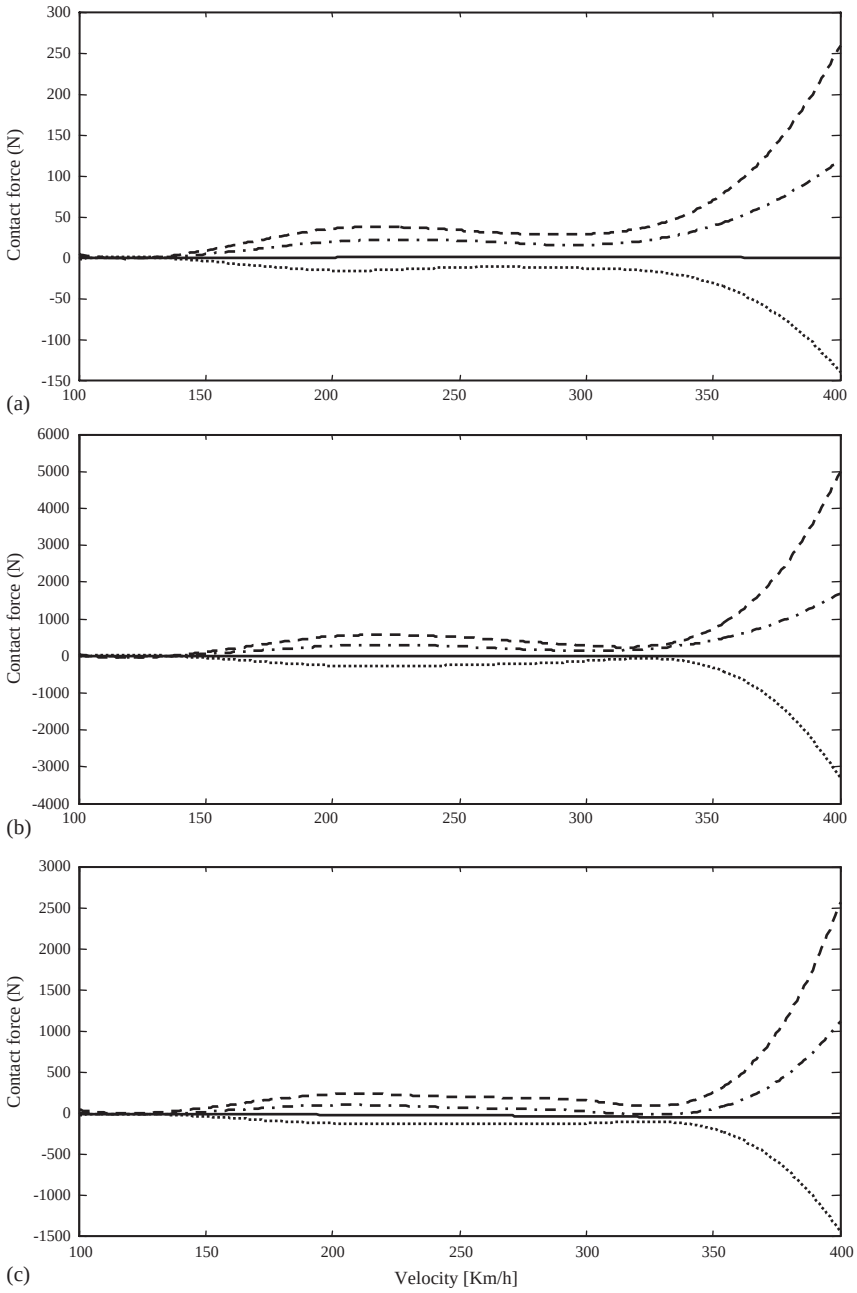

Fig. 10. Contact force sensitivity with respect to mass. Max–Min (—), Max (·), Min (···), average (—); (a) contact force for m_1; (b) contact force for m_2; and (c) contact force for m_3.

dominant design variable is determined from the results. Standard deviation and average of the contact force are mainly considered because of vibration with high frequency as the vehicle velocity increases.

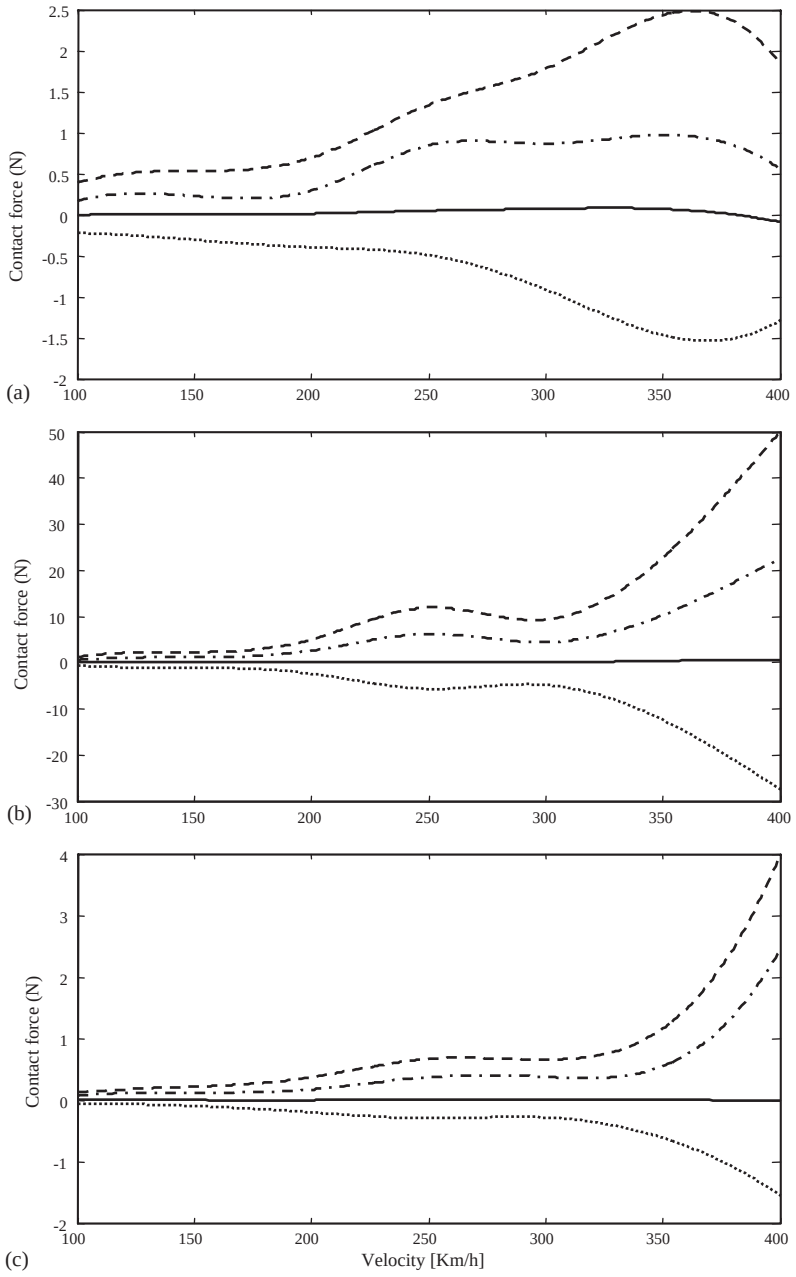

Fig. 11. Contact force sensitivity with respect to damper. Max–Min (- - -), Max (·), Min (···), average (—); (a) contact force for c_1; (b) contact force for c_2; and (c) contact force for c_3.

4.1. Effects of the design variables

The effects of the design variables on state sensitivity are considered in the time domain. Fig. 10 shows the results of sensitivity analysis of the average contract force with respect to the three masses. It shows that the sensitivity of the average contact force has constant values and variance increases for vehicle speed by mass m_1, m_2 and m_3. Mass m_1 has comparatively smaller values than m_1 and m_2.

Fig. 11 Shows the results of the sensitivity analysis of the average contract force with respect to the three dampers. It shows that the sensitivity of the average contact force for vehicle speed is affected by c_2. Other dampers, c_1 and c_3 affect contact force, but c_1 and c_3 have small sensitivity analysis values compared with c_2.

Fig. 12 shows the results of sensitivity analysis of the average contract force with respect to the three stiffnesses. It shows that the sensitivity of the average contact force for vehicle speed is mainly k_3. The sensitivity of k_3 stiffness increases as the vehicle velocity increases.

Fig. 12 shows that the sensitivity of the average contact force for vehicle speed is affected by k_2. Other stiffnesses, k_1 and k_3 affect contact force, but k_1 and k_3 have small sensitivity analysis values when compared with k_2.

4.2. Dominant design variables

Dominant design variables can be examined based on state sensitivity analyses. In order to check dominant design variables, a normalization process is required for dimension matching. In this research, a 1% perturbation is performed for this process. Rank of the design variables vary as the vehicle speed is increased.

Fig. 13 shows the average contact force for normalized design variables. Contact loss occurs when average contact is a negative value. Fig. 14 shows the standard deviation of contact force for the normalized design variables. From the results of Figs. 13 and 14, the variation and average of contact force at high speed is affected by design variables, mass m_3, mass m_2, damper c_1, and stiffness k_1. Damper c_3 and stiffness k_3 hardly affect contact force under the conditions as they have constant values for the up lifting and aero forces.

4.3. Modified design variable

Through sensitivity analysis, the design variables m_3, m_2, c_1 and k_1 should be modified for improving the performance of the pantograph. In this study, the design values, mass m_2, mass m_3 and stiffness k_1 were modified to improve contact loss ratio.

Figs. 15–17 show standard deviation of each displacement changing the design values m_3, m_2, and k_1. The gray lines are the values of the early pantograph.

The standard deviation of each displacement should have values because the smaller deviation of the pantograph vibration has a constant contact force. From this point of view, the values of design variables maintaining a small value of the standard deviation were chosen.

Fig. 18 shows the results of the contact loss ratio between the early pantograph model and the modified pantograph with sensitivity analysis. The contact loss ratio improved remarkably by modifying design variables.

Fig. 19 shows the result of the contact loss velocity between the early pantograph model and the modified pantograph as the sensitivity analysis. The modified pantograph is almost completely devoid of contact loss because the maximum value is larger than the difference between the

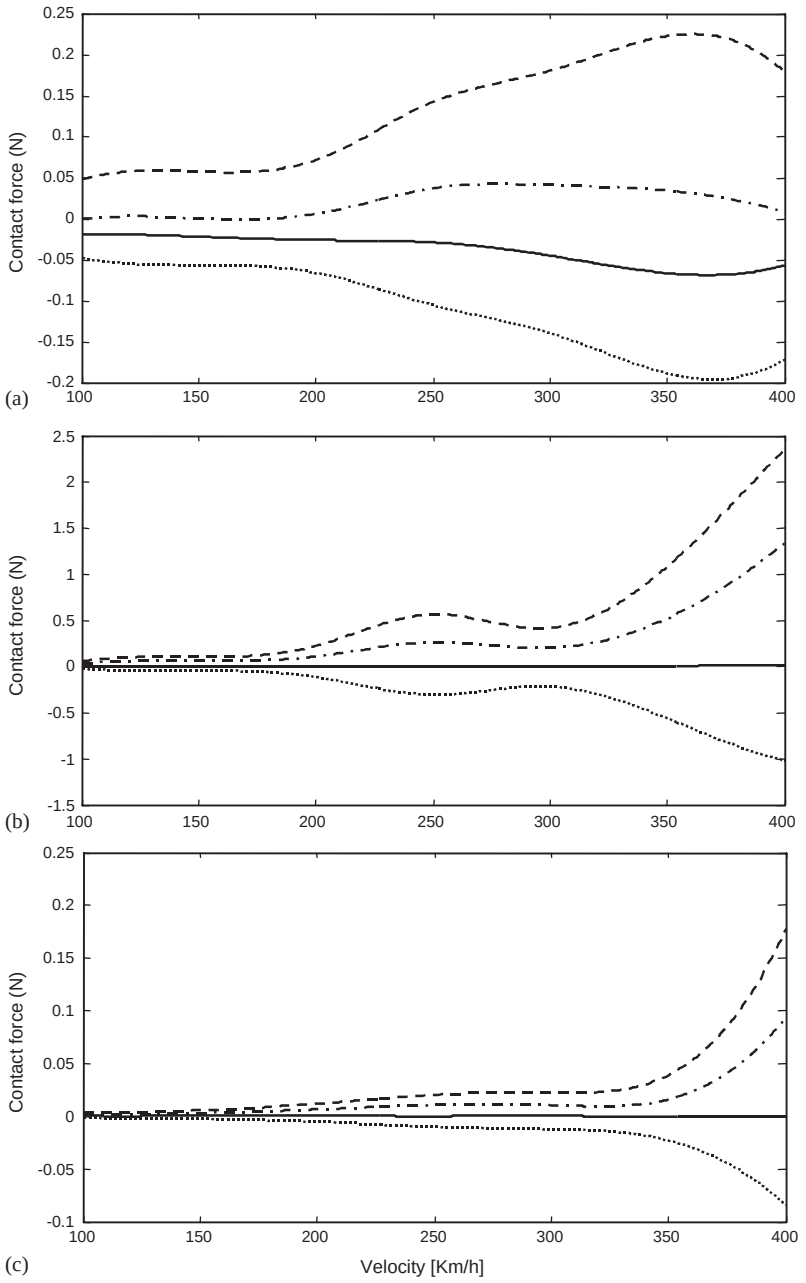

Fig. 12. Contact force sensitivity with respect to stiffness. Max–Min (- - -), Max (·), Min (···), average (—); (a) contact force for k_1; (b) contact force for k_2; and (c) contact force for k_3.

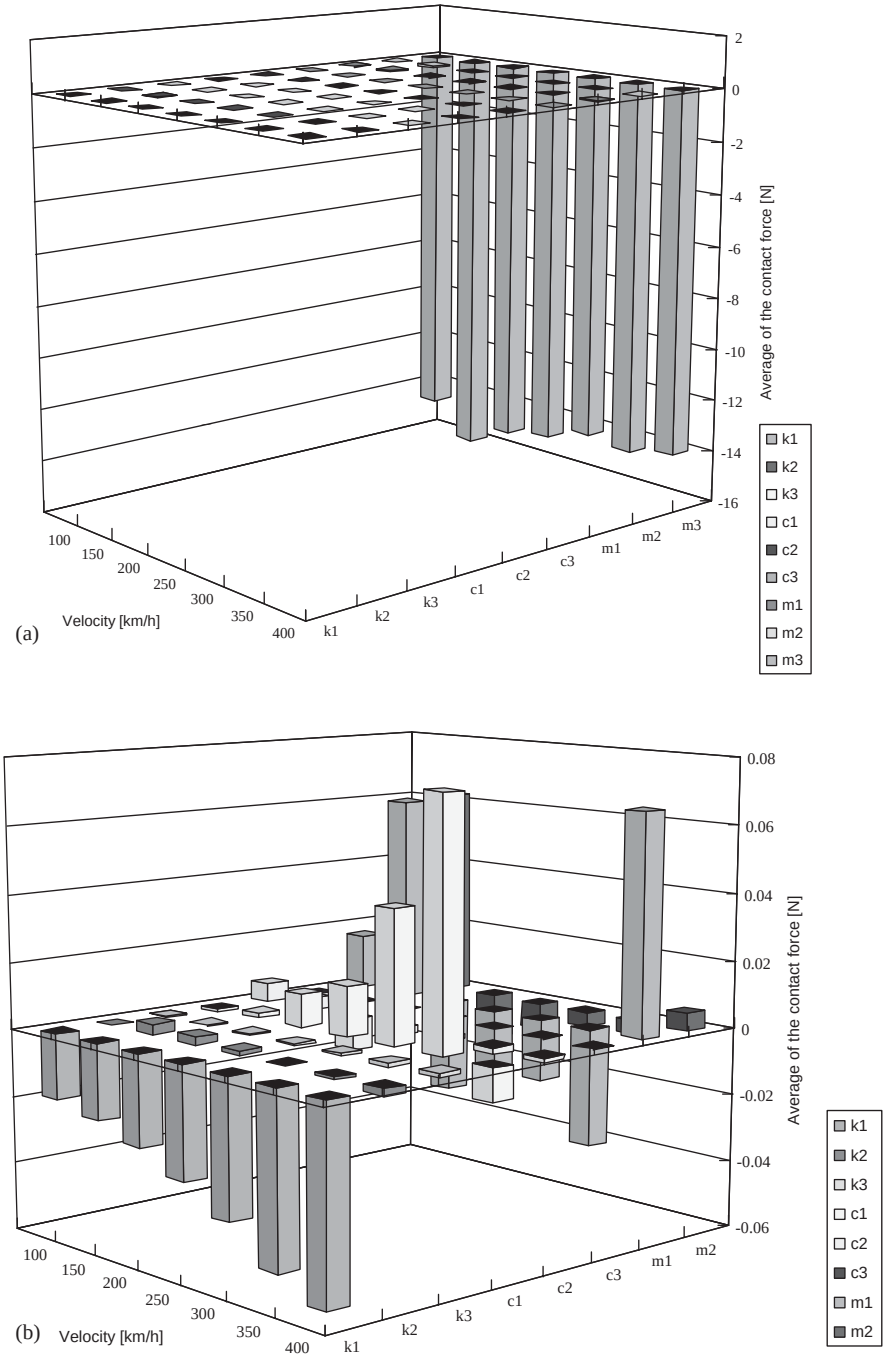

Fig. 13. Average value of normalizing sensitivity with respect to design variables: (a) all design variables and (b) design variables except m_3.

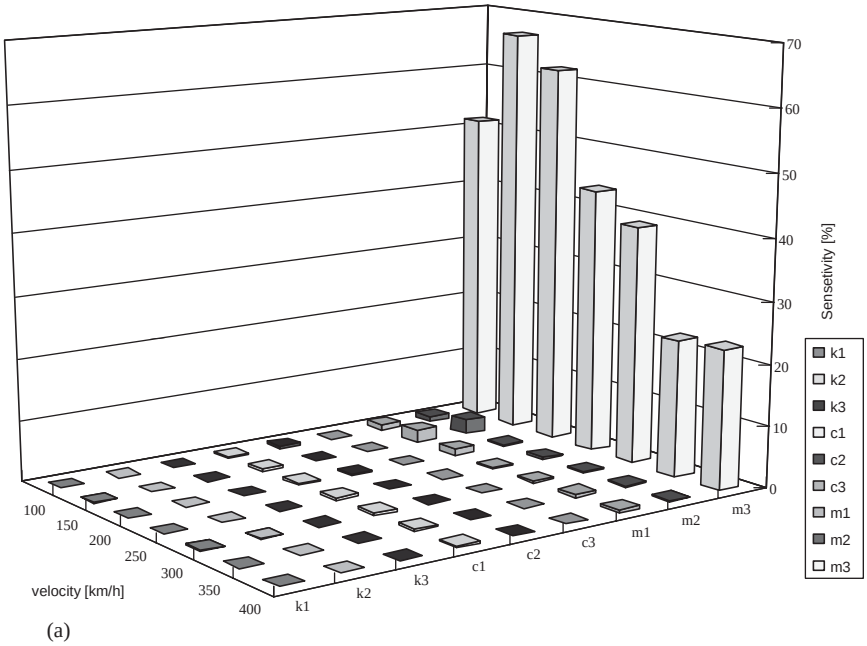

(a)

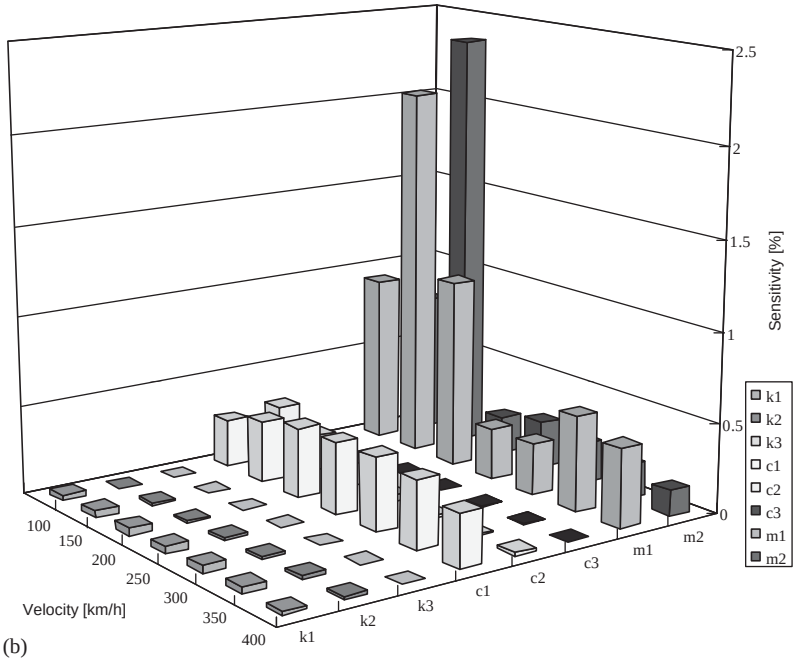

(b)

Fig. 14. Standard deviation of normalizing sensitivity with respect to design variables: (a) all design variables (b) design variables except m_3.

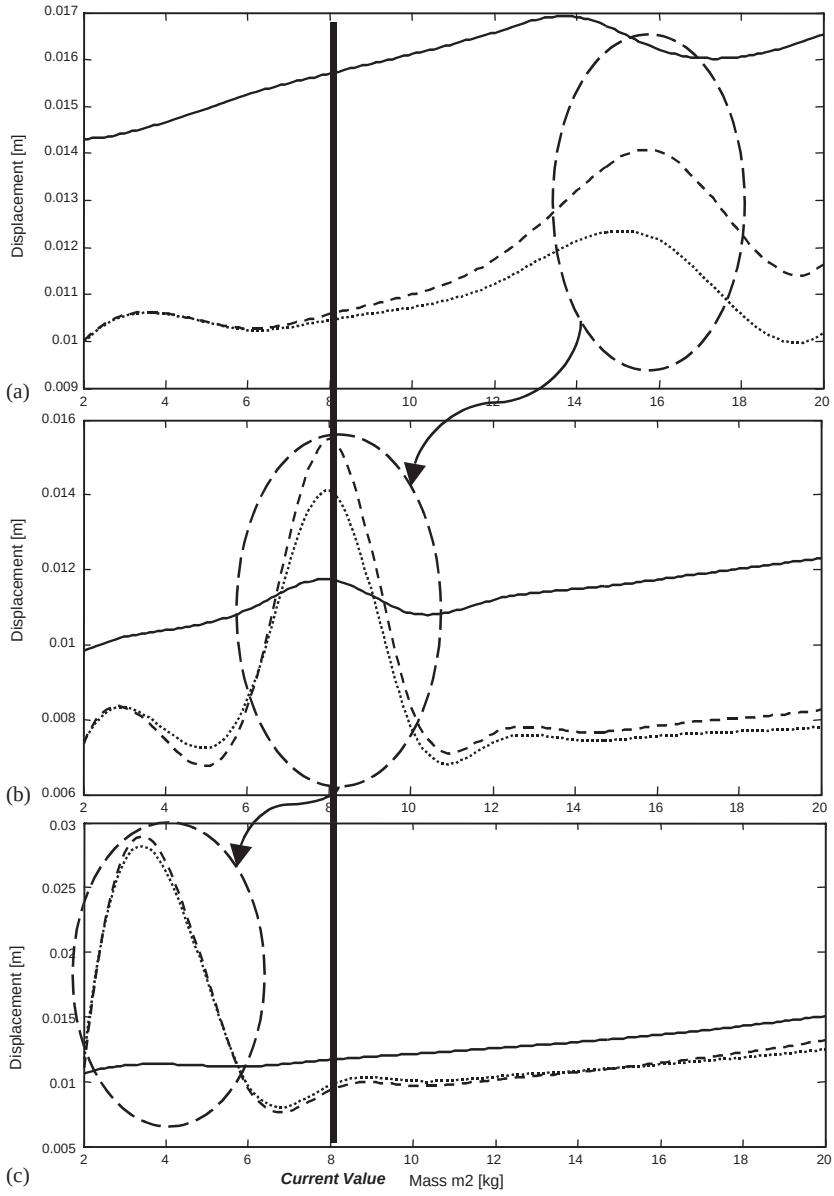

Fig. 15. Standard deviation of the pantograph displacements for mass m_2 by frequency inputs y_1 (—), y_2 (- - -), y_3 (···): (a) 8.73 Hz; (b) 10.9 Hz; and (c) 13.3 Hz.

maximum and the minimum at the 100–400 km/h velocity interval. Figs. 18 and 19 show the possibility of improving not only the contact loss ratio, but also the velocity of the contact loss by modifying design variables.

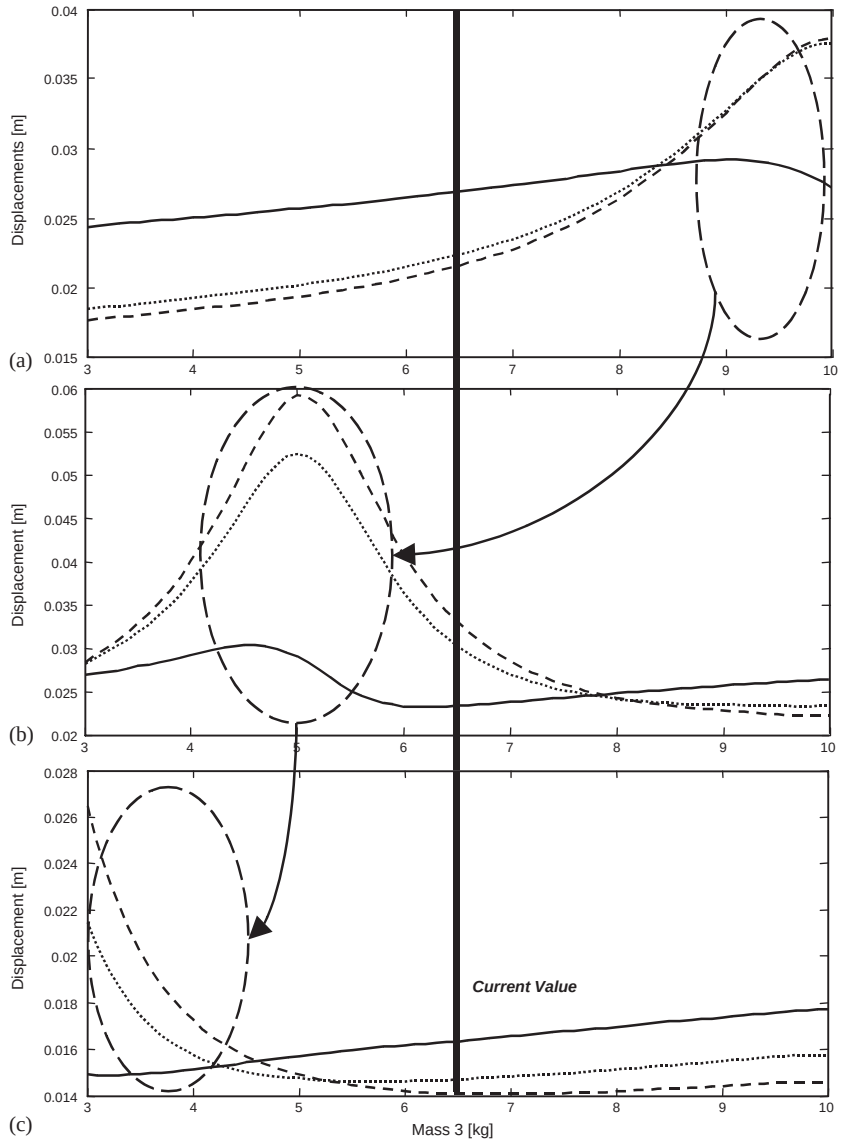

Fig. 16. Standard deviation of the pantograph displacements for mass m_3 by frequency inputs y_1 (—), y_2 (- - -), y_3 (···): (a) 9.7 Hz; (b) 11.1 Hz; and (c) 12.2 Hz.

5. Conclusions

In this study, dynamic performance is analyzed by the sensitivity of the pantograph. First, the pantograph–catenary system is analyzed by FEM analysis. As contact force was the main factor for pantograph performance, contact force has been analyzed. The uplift and aero forces were assumed to be constant values. From various sensitivity analyses, useful sensitivity information is

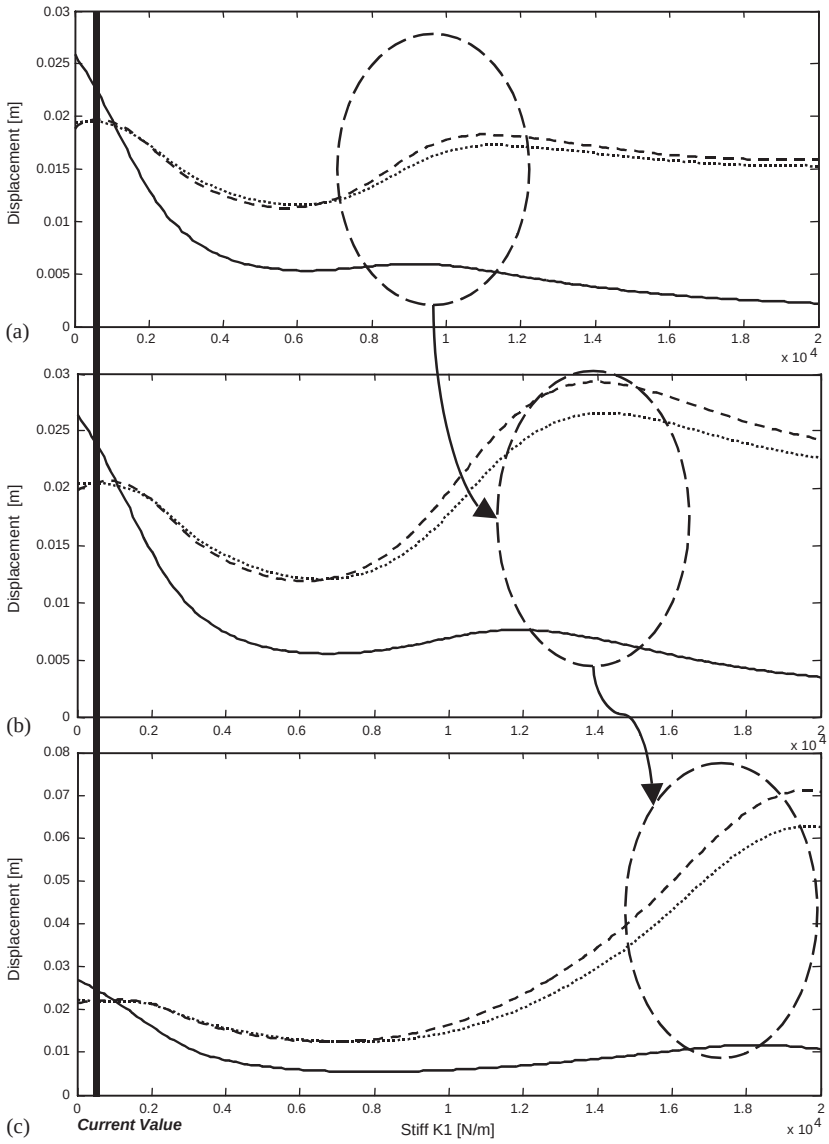

Fig. 17. Standard deviation of the pantograph displacements for stiffness k_1 by frequency inputs. y_1 (—), y_2 (- - -), y_3 (···); (a) 9.14 Hz; (b) 9.41 Hz; and (c) 9.69 Hz.

evaluated at various velocities with respect to design variables. The pantograph could be improved by modifying the design variables through sensitivity analysis.

The conclusions of this paper are as follows:

1. Considering the responses at high speed, the contact wire and the messenger wire were modelled as beams with bending stiffness and tension.
2. Catenary was analyzed using FEM with beam modelling.

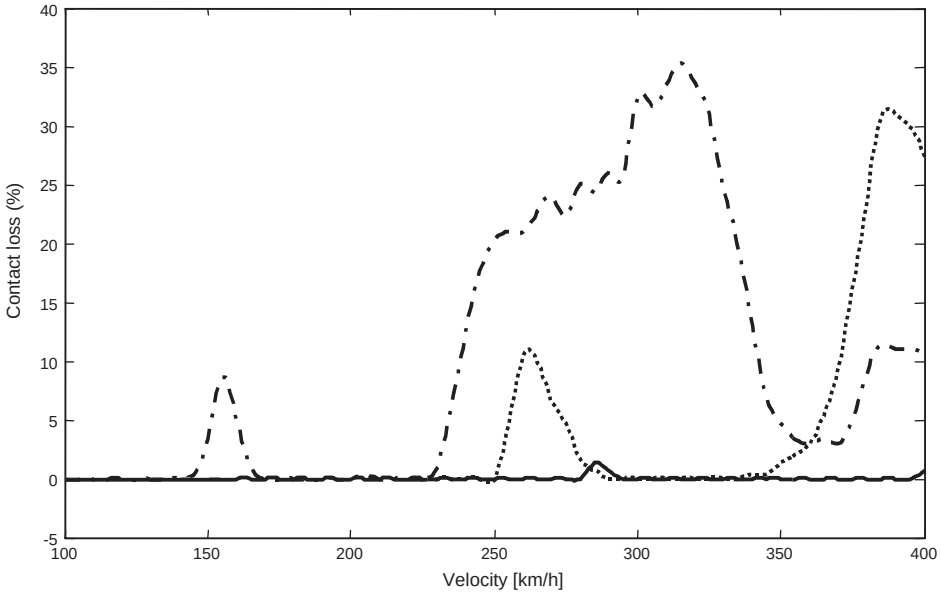

Fig. 18. Comparison of the contact loss ratio of the different pantograph cases: initial model (–·–), improving design variable m_3 (···), improving design variables m_3, m_2, k_1 (—).

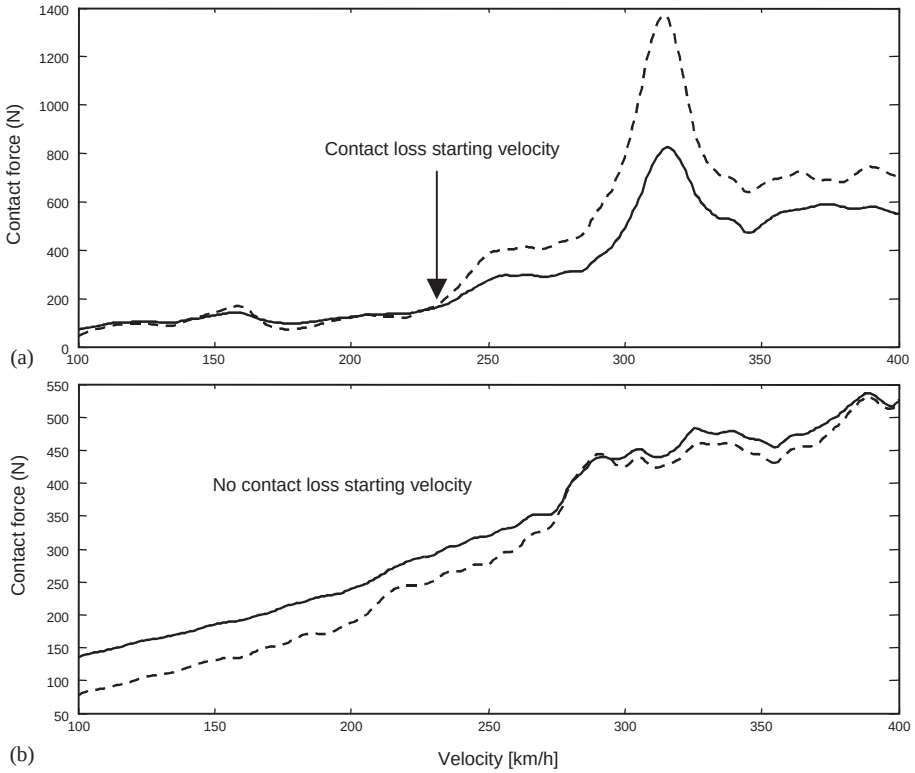

Fig. 19. Comparison of contact loss occurrence velocities. Max–Min (- - -), Max (—); (a) before improving the design variables, and (b) after improving design variables.

3. The stiffness function from the FEM analysis of catenary was applied to the pantograph dynamics and sensitivity analysis.
4. The pantograph dynamic equations are derived for applying sensitivity analysis and verified by experiment results.
5. Through sensitivity analysis for contact force, design variables were modified to reduce contact loss.
6. The pantograph performance could be improved from the modified design variables.

Acknowledgements

This study was supported by a grant of the International Mobile Telecommunications 2000 R&D Project, Ministry of Information & Communication, Republic of Korea.

Appendix A. Sensitivity formulations

Sensitivity functions for RHS terms of Eq. (16) are derived as follows with nine sensitivity equations for each design variable obtained from partial derivative operation with respect to design variables:

(1) For $b_1 = m_1$:

$$\mathbf{f}_{b_1} = \begin{bmatrix} 0 \\ \dfrac{k_1+k_2}{m_1^2}x_1 + \dfrac{c_1+c_2}{m_1^2}x_2 - \dfrac{k_3}{m_1^2}x_3 - \dfrac{c_2}{m_1^2}x_4 - \dfrac{F_L}{m_1^2} \\ 0 \\ 0 \\ 0 \\ 0 \end{bmatrix}. \tag{A.1}$$

(2) For $b_2 = m_2$:

$$\mathbf{f}_{b_2} = \begin{bmatrix} 0 \\ 0 \\ 0 \\ -\dfrac{k_2}{m_2^2}x_1 - \dfrac{c_2}{m_2^2}x_2 + \dfrac{k_2+k_3}{m_2^2}x_3 + \dfrac{c_2+c_3}{m_2^2}x_4 - \dfrac{k_3}{m_2^2}x_5 - \dfrac{c_3}{m_2^2}x_6 - \dfrac{F_2}{m_2^2} \\ 0 \\ 0 \end{bmatrix}. \tag{A.2}$$

(3) For $b_3 = m_3$:

$$\mathbf{f}_{b_3} = \begin{bmatrix} 0 \\ 0 \\ 0 \\ 0 \\ 0 \\ -\dfrac{k_3}{m_3^2}x_3 - \dfrac{c_3}{m_3^2}x_4 + \dfrac{k_3 + K(t)}{m_3^2}x_5 - \dfrac{c_3}{m_3^2}x_6 - \dfrac{F_3}{m_3^2} \end{bmatrix}. \tag{A.3}$$

(4) For $b_4 = c_1$:

$$\mathbf{f}_{b_4} = \begin{bmatrix} 0 \\ -\dfrac{x_2}{m_1} \\ 0 \\ 0 \\ 0 \\ 0 \end{bmatrix}. \tag{A.4}$$

(5) For $b_5 = c_2$:

$$\mathbf{f}_{b_5} = \begin{bmatrix} 0 \\ -\dfrac{x_2}{m_1} + \dfrac{x_4}{m_1} \\ 0 \\ \dfrac{x_2}{m_2} - \dfrac{x_4}{m_2} \\ 0 \\ 0 \end{bmatrix}. \tag{A.5}$$

(6) For $b_6 = c_3$:

$$\mathbf{f}_{b_6} = \begin{bmatrix} 0 \\ 0 \\ 0 \\ -\dfrac{x_4}{m_2} + \dfrac{x_6}{m_2} \\ 0 \\ \dfrac{x_4}{m_3} - \dfrac{x_6}{m_3} \end{bmatrix}. \tag{A.6}$$

(7) For $b_7 = k_1$:

$$\mathbf{f}_{b_7} = \begin{bmatrix} 0 \\ -\dfrac{x_1}{m_1} \\ 0 \\ 0 \\ 0 \\ 0 \end{bmatrix}. \tag{A.7}$$

(8) For $b_8 = k_2$:

$$\mathbf{f}_{b_8} = \begin{bmatrix} 0 \\ -\dfrac{x_1}{m_1} + \dfrac{x_3}{m_1} \\ 0 \\ \dfrac{x_1}{m_2} - \dfrac{x_3}{m_2} \\ 0 \\ 0 \end{bmatrix}. \tag{A.8}$$

(9) For $b_9 = k_3$:

$$\mathbf{f}_{b_9} = \begin{bmatrix} 0 \\ 0 \\ 0 \\ -\dfrac{x_3}{m_2} + \dfrac{x_5}{m_2} \\ 0 \\ \dfrac{x_3}{m_3} - \dfrac{x_5}{m_3} \end{bmatrix}. \tag{A.9}$$

Appendix B. Nomenclature

m_1 mass of the pantograph frame
m_2 mass of the pantograph plunger
m_3 mass of the pantograph panhead
c_1 damping coefficient between the vehicle body and the frame
c_2 damping coefficient between the frame and the plunger
c_3 damping coefficient between the plunger and the panhead
k_1 stiffness coefficient between the vehicle body and the pantograph frame

k_2 stiffness coefficient between the frame and the plunger
k_3 stiffness coefficient between the plunger and the panhead
F_L static uplift force of the pantograph
F_2, F_3 aerodynamic uplift force
m_m mass of the messenger wire element
m_c mass of the contact wire element
EI_m bending stiffness of the messenger wire
EI_c bending stiffness of the contact wire
T_m tension of the messenger wire
T_c tension of the contact wire
u_m displacement of the messenger wire element
u_c displacement of the contact wire element
k_d equivalent stiffness of the dropper
k_s equivalent stiffness of the support tower

References

[1] J.H. Jang, C.S. Han, The state sensitivity analysis of the front wheel steering vehicle: in the time domain, KSME International Journal 11 (1997) 595–604.
[2] A. Balestrino, O. Bruno, A. Landi, L. Sani, Innovative solutions for overhead catenary–pantograph system: wire actuated control and observed contact force, Vehicle System Dynamic 33 (2000) 69–89.
[3] C.N. Jensen, H. True, S. Consult, Dynamic of an electrical overhead line system and moving pantographs, Vehicle System Dynamic 28 (1998) 104–113.
[4] D.N. O'Connor, S.D. Eppinger, W.P. Seering, D.N. Wormley, Active control of a high-speed pantograph, Journal of Dynamic Systems, Measurement, and Control 119 (1997) 1–4.
[5] G. Diana, F. Fossati, F. Resta, High speed railway: collecting pantographs active control and overhead lines diagnostic solutions, Vehicle System Dynamic 30 (1998) 69–84.
[6] K. Manabe, Periodical dynamic stabilities of a catenary–pantograph system, Quarterly Report of Railway Technical Research Institute 35 (1994) 112–117.
[7] T.X. Wu, M.J. Brennan, Basic analytical study of pantograph–catenary system dynamics, Vehicle System Dynamic 30 (1998) 443–456.
[8] T.X. Wu, M.J. Brennan, Dynamic stiffness of a railway overhead wire system and its effect on pantograph–catenary system dynamics, Journal of Sound and Vibration 219 (1999) 483–502.
[9] T. Yagi, A. Stensson, C. Hardell, Simulation and visualization of the dynamic behavior of an overhead power system with contact breaking, Vehicle System Dynamic 25 (1996) 31–49.
[10] T. Vinayagalingam, Computer evaluation of controlled pantographs for current collection from simple catenary overhead equipment at high speed, American Society of Mechanical Engineers, Journal of Dynamics Systems, Measurement, and Control 105 (1983) 287–294.
[11] J.R. Ockendon, A.B. Tayor, The dynamics of a current collection system for an electric locomotive, Proceedings of the Royal Society of London A 211 (1971) 336–357.
[12] E.J. Haug, V.N. Sohoni, Design sensitivity analysis and optimization of kinematically driven systems, in: E.J. Haug (Ed.), Computer Aided Analysis and Optimization of Mechanical System Dynamics, NATO ASI Series F: Computer and System Sciences, Vol. 9, Springer, Berlin, pp. 499–554.
[13] C.N. Vanderplaats, Numerical Optimization Techniques for Engineering Design with Applications, McGraw-Hill, New York, 1984.
[14] J.S. Arora, Introduction to Optimum Design, McGraw-Hill, New York, 1989.